Article

Towards Deeper Measurements of Tropical Reefscape Structure Using the WorldView-2 Spaceborne Sensor

Antoine Collin [1],* and James L. Hench [2]

[1] USR 3278 CRIOBE CNRS-EPHE, BP 1013, Papetoai, Moorea 98729, French Polynesia

[2] Nicholas School of the Environment, Duke University, 135 Marine Lab Road, Beaufort, NC 28516, USA; E-Mail: jim.hench@duke.edu

* Author to whom correspondence should be addressed; E-Mail: antoinecollin1@gmail.com; Tel.: +689-56-1345.

Abstract: Owing to the shallowness of waters, vast areas, and spatial complexity, reefscape mapping requires Digital Depth Models (DDM) at a fine scale but over large areas. Outperforming waterborne surveys limited by shallow water depths and costly airborne campaigns, recently launched satellite sensors, endowed with high spectral and very high spatial capabilities, can adequately address the raised issues. Doubling the number of spectral bands, the innovative eight band WorldView-2 (WV2) imagery is very susceptible to enhance the DDM retrieved from the traditional four band QuickBird-2 (QB2). Based on an efficiently recognized algorithm (ratio transform), resolving for the clear water bathymetry, we compared DDM derived from simulated QB2 with WV2 spectral combinations using acoustic ground-truthing in Moorea (French Polynesia). Three outcomes emerged from this study. Increasing spatial resolution from 2 to 0.5 m led to reduced agreement between modeled and *in situ* water depths. The analytical atmospheric correction (FLAASH) provided poorer results than those derived without atmospheric correction and empirical dark object correction. The purple, green, yellow and NIR3 (WV2 1st-3rd-4th-8th bands) spectral combination, processed with the atmospheric correction at the 2 m resolution, furnished the most robust consistency with ground-truthing (30 m ($r = 0.65$)), gaining 10 m of penetration relative to other spaceborne-derived bathymetric retrievals. The integration of the WV2-boosted bathymetry estimation into radiative transfer model holds great promise to frequently monitor the reefscape features at the colony-scale level.

1. Introduction

Many tropical reefscape ecological processes are intricately linked with bathymetry and bathymetric gradients. Characterizing the structure and monitoring changes in coral ecosystems requires accurate information on water depth [1]. Knowledge of the bathymetry at various spatial scales constitutes a cornerstone of the tropical reefscape ecology. When focused on the ecological processes related to community-scale, very high spatial resolution Digital Depth Models (DDM) are necessary to render features such as coral bommies or thickets over reef flats, reef crest, and spur-and-groove topography.

In open water, sonar measurements have allowed benthic habitat to be evaluated from the abyssal landscape to the littoral fringe. However, waterborne systems have limited capacity to perform surveys over shallow coral reefs. Moreover, they can be difficult mobilize in remote areas and for repeated surveys to study seasonal changes. Bathymetric Light Detection And Ranging (LiDAR) measurements are well suited to surveying both land and shallow waters simultaneously [2] but can be prohibitively expensive, particularly in remote coral reef islands and atolls. Although LiDAR technology delivers DDM at a 0.25 m vertical accuracy, the horizontal accuracy is usually 5 m, but can attain 2 m at high prices, often making it cost-prohibitive. Very high resolution (VHR) mapping can also be obtained either by multispectral spaceborne imagery (QuickBird-2; QB2 hereafter) or hyperspectral airborne acquisition (Compact Airborne Spectrographic Imager). The hyperspectral mapping of reef bathymetry has been successful across a range sites including Hawaii [3], the Bahamas [4], and Honduras [5]. These studies have all exploited knowledge of water depth to assess benthic chromatism (visible albedo), enhancing habitat mapping [6,7]. Providing very high spectral resolution with more than 200 narrow bands, the hyperspectral method permitted improvements to bathymetry retrieval and discrimination of coral pigments. However the long-term planning and associated costs undermines its utility for campaigns over large or remote reefs ecosystems. Since the launch of the QB2 sensor in 2001, spaceborne passive remote sensing has become a valuable tool for retrieving water depth at a spatial scale relevant to community processes [6,8–10].

Passive remote sensors over reefscapes measure reflected sunlight that attenuates exponentially with water depth. This exponential decay rate is proportional to the wavelength involved. The radiative transfer model developed by Lyzenga [11] showed that two bands could provide a good estimate of the water depth. Improvements to the radiative transfer model integrated effects induced by variations in water clarity [12], although this effect can be comparatively small in oligotrophic waters found on many tropical reefscapes. Based on a variation of this empirical linear model, the detection of water depths from 18 to 20 m by QB2 imagery has been satisfactorily achieved on coral reefscapes [6,13]. Lee *et al.* [14] developed a non-linear optimization of a semi-analytical model, which has been used to retrieve water depths up to 20 m from a QB2 acquisition over Kanehoe Bay in Hawaii [9]. Nevertheless, the latter assessment required simplification of the semi-analytical algorithm, which is rather dedicated to hyperspectral approaches, lying beneath the purpose of this paper. Solving the empirical model necessitates finding five unknowns that have to be measured *in situ* or derived from

published measurements. Such tuning can raise substantial logistical issues particularly for very shallow and remote areas where benthic and water column parameters can be strongly problematic to elucidate. In delving into the mapping of relatively large and remote reefscape regions, Stumpf *et al.* [15] proposed an alternative empirical method that only requires one tunable constant. Based on an algorithm involving a ratio transform between two bands, the bathymetry has been reliably resolved up to approximately 20 m in clear water (northwestern Hawaiian islands). However, this work was applied to an IKONOS imagery, delivering four bands at four meter spatial resolution, that is susceptible to smoothing of ecological heterogeneity occurring at the community-level scale.

Refining the QB2 spatial resolution, the WorldView-2 (WV2 hereafter) system collects data at 1.84 m at nadir (*versus* 2.62 m for QB2) but doubles the QB2 spectral abilities providing five visible bands, from purple to red, and three near-infrareds (Table 1). One might expect that the purple band, offering the highest water penetration of the VHR spaceborne remote sensing, to potentially increase the limit of the water depth that can be extracted. In this study, the ratio transform developed by Stumpf *et al.* [15] was applied to WV2 data of a reefscape on the island of Moorea (Society Islands archipelago, French Polynesia, Figure 1). The model was employed to estimate the bathymetry as a function of the spectral bands and atmospheric correction. To increase spatial resolution to the grain-size where colony-related processes are of importance, pansharpened data (0.5 m) were also evaluated with respect to both previous modalities. The effectiveness of the method was evaluated by comparison between depths retrieved from WV2 imagery and ground-truth depths acquired by a waterborne digital sonar acoustic system. The contribution of the new WV2 spectral bands to the enhancement of the bathymetry estimation and the benefits to understanding reefscape ecology stemming from these novel findings are then discussed.

Table 1. Spectral characteristics of the two best Very High Resolution spaceborne sensors, Worldview-2 (WV2) and QuickBird-2 (QB2).

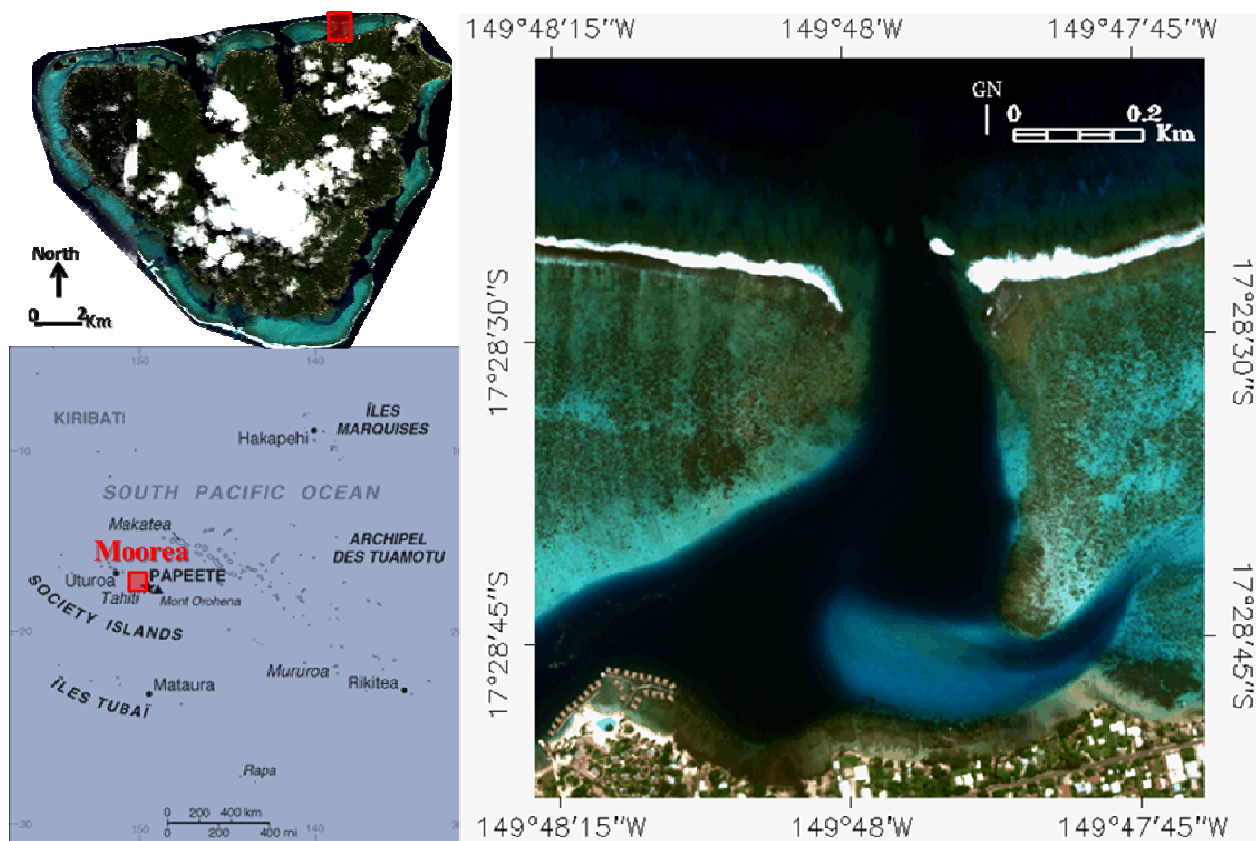| Waveband Colours	Waveband Numbers	Waveband Names	WV2 Wavelength Range (nm)	QB2 Wavelength Range (nm)
Purple	1	"Coastal blue"	400–450	
Blue	2	Blue	450–510	450–520
Green	3	Green	510–580	520–600
Yellow	4	Yellow	585–625	
Red	5	Red	630–690	630–690
NIR1	6	"Red edge"	705–745	
NIR2	7	Near InfraRed 1	770–895	760–890
NIR3	8	Near InfraRed 2	860–1040	
		Panchromatic	450–800	450–900

2. Methodology

2.1. Study Area

The study site was located in a coral reef lagoon along the northeastern coast of Moorea (17°47′S, 149°80′W), a 1.2 million-year-old volcanic island in the Society Islands of French Polynesia. Moorea

is located to the north-west of Tahiti, separated by a channel 17 km wide and 1,800 m deep. Moorea is an example of an intermediate state in the genesis of a tropical volcanic island issued from a geological hotspot, and a representative case of the range of bathymetric features usually met in tropical reefscapes. Containing fringing and barrier reefs as well as vegetated subaerial islets (vernacularly called *motu*) the shallow water areas of this island can significantly affect the circulation in the system [16], and many related ecological questions. To date, the reefs in Moorea have been poorly mapped. The only previous bathymetric measurements were made by the French *Service Hydrographique et Océanographique de la Marine* (*SHOM*) to produce very coarse resolution charts for navigation, with large areas simply marked "reef". This situation is not uncommon for many shallow water reef complexes in French Polynesia and elsewhere.

Figure 1. Location of study area on the north shore of Moorea, Society Island archipelago, French Polynesia, and color image of study area. The study area encompassed Irahonu Pass, outer, barrier and fringing reefs and a sand bank.

Extending over 1.22 km^2, the study area encompassed a great variety of geomorphic features, ranging from consolidated habitats, including outer reefs, reef crest, barrier and fringing reefs, to clastic sediments found in the pass and the channel. These latter banks were composed of gravel-sand from coral erosion. Areas with fine grain-size, appear to have stronger visual reflectance (e.g., the bank located in the southeastern region of the study area in Figure 1). The outer reef was significantly impacted by two major events, namely the 2006–2009 crown-of-thorns seastar (*Acanthaster planci*) outbreak [17] and Cyclone Oli in February 2010 [10], resulting in grayish pavement and coral rubble colonized by very sparse *Pocillopora* sp.-dominated coral communities. The reef crest is typically
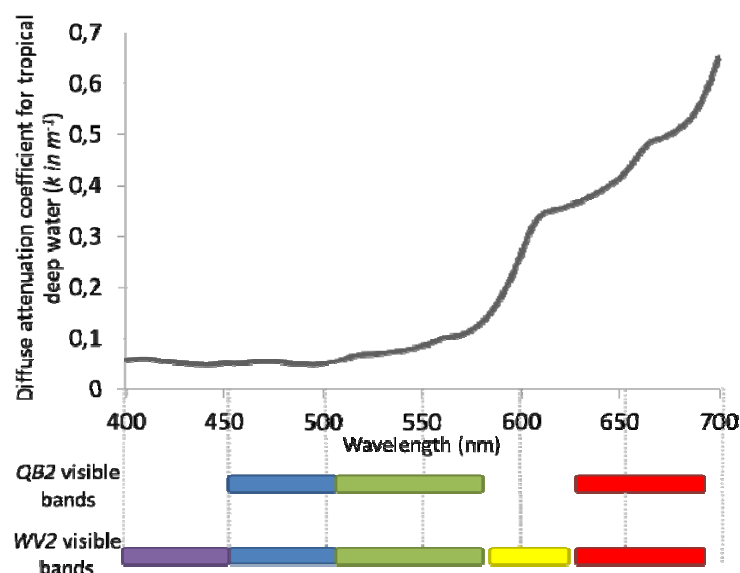
covered with brown macro-algae (*Turbinaria* sp.). Sheltered in the lagoon, massive stony corals, mainly represented by brown/yellow *Porites* sp. and brown/yellow branching corals such as *Synarea rus*. The larger coral colonies can be topped by red coralline algae and *Turbinaria* sp., green algae (*Halimeda* sp.), or filamentous turf algae when the entire colony was dead. While the seaward slope of the fringing reef was primarily populated by *S. rus*, the middle part was pavement, colonized by red encrusting algae and tufts of brown algae (*Padina* sp.).

2.2. Image Acquisition and Processing

2.2.1. WorldView-2 Spaceborne Multispectral Data

Spaceborne multispectral imagery was acquired on 17 March 2010 over Moorea with the WV2 instrument. Launched in October 2009 by DigitalGlobe, WV2 uses an eight band multispectral dataset with a 1.84 m spatial resolution and a panchromatic dataset with 0.46 m spatial resolution when viewing at nadir. Given the off-nadir viewing angle was 19° during the acquisition, the imagery was resampled at 2 and 0.5 m spatial resolution for multispectral and panchromatic datasets, respectively. The dual-sensor can collect a 16.4 km swath up to a 250 km length with 11 bit radiometric resolution. For the sake of comparison, the Quickbird-2 imagery was resampled at 2 and 0.5 m, respectively. Comparing specifications of WV2 and its predecessor in terms of the VHR sensor leader, QB2, allows the technological leap to be quantified. Although the length of the scene was diminished by 100 km, the refinement in spatial resolution (gaining 0.78 and 0.19 m in multispectral and panchromatic modes, respectively) and the doubling of the spectral capabilities (from four to eight) hold great promise to characterize tropical reefscape features at a spatial scale suitable for elucidating reef changes down to the scale of large coral colonies. Of special relevance is the purple band (or "coastal band") which is expected to provide benthic information at a greater depth than the blue band given its inherently increased water penetration characteristics (Figure 2).

Figure 2. Visible spectral capabilities of the two Very High Resolution Sensors, Quickbird-2 (QB2) and WorldView-2 (WV2), related to the diffuse attenuation coefficient estimated for Moorea's tropical waters (modified from [18]).

Since the water surface and water column did not have significant roughness or plume, the glint-removal procedure was circumvented and we assumed that the water column was sufficiently homogeneous over the entire scene to apply the following model of bathymetry retrieval without weighting regions within the study area. However, prior to carrying out the analysis, two corrections were applied using the image processing software IDL-ENVI (Research Systems, Inc.). A geometric correction was applied using the metadata describing the sun-sensor-scene geometry (.rpb file) and geolocalized ground control points readily identifiable on the imagery. The warping model (nearest neighbor), implemented only where the GCP whose Root Mean Square Errors were ≤0.5 m, was fitted with a second order polynomial to correct elementary non-linear projection errors. Also, the at-sensor radiance calibration permitted the 11-bit digital values to be converted into physically meaningful units (in $W \cdot m^{-2} \cdot sr^{-1}$) using the band-related coefficients (contained in the .imd file).
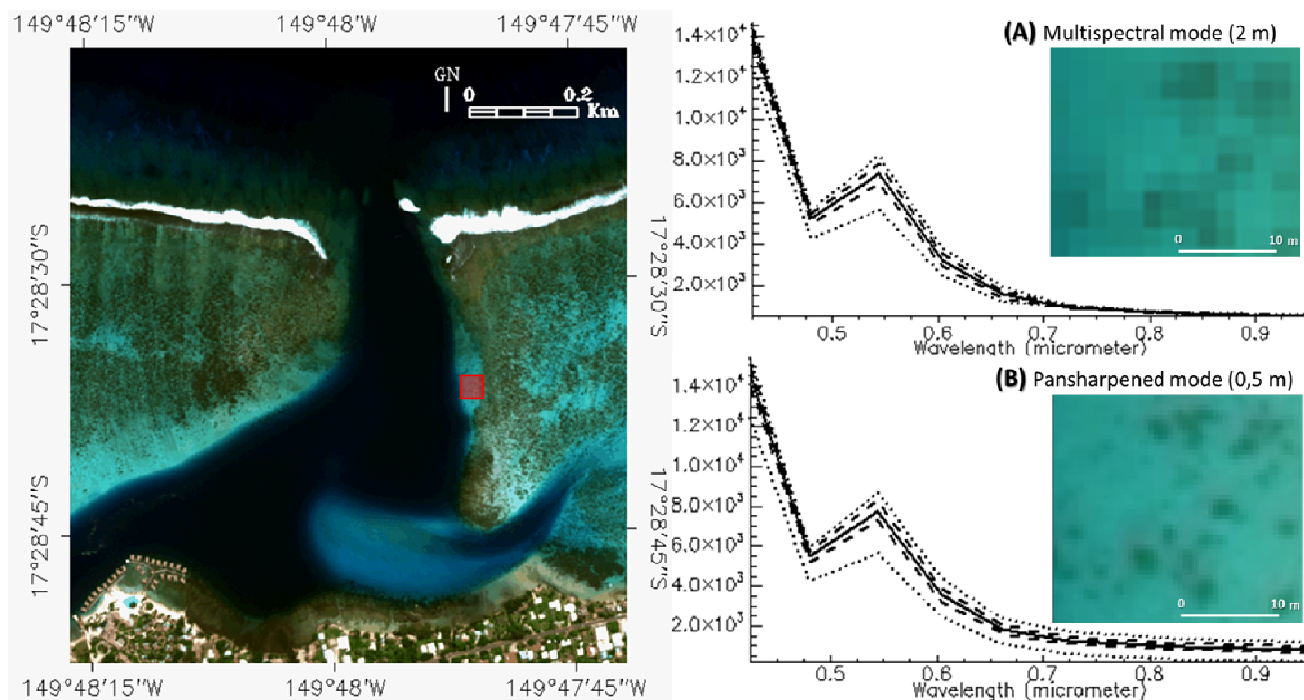
2.2.2. Pansharpening

Pansharpening is an image fusion method in which low spatial resolution multispectral data are fused with higher spatial resolution panchromatic data to build a multispectral high-resolution dataset. Even though the spectral response to a pansharpened pixel (or sub-pixel) cannot be refined, the textural information benefits from a fourfold increase in our study (from 2 to 0.5 m). The consensus view of image processing scientists is that the Gram-Schmidt (GS) algorithm outperforms other transformations such as Principal Components or Color Normalized spectral sharpening, because it relies on the spectral response function of the specific sensor to simulate the low-resolution panchromatic image [19]. A series of five steps were carried out, according to Laben and Brover [20]: (a) simulating a low-resolution panchromatic image using the WV2 spectral response function; (b) performing a GS transformation on the previous simulated band, set as the first band, as well as the other eight low-resolution bands; (c) adjusting the histogram of the initial panchromatic image to match the first GS-transformed band; (d) substituting the adjusted initial panchromatic image for the first GS-transformed band; and finally, (e) inverse GS, transforming the new set of transform bands to produce the enhanced spatial resolution multispectral digital image.

Given the trade-off between the surplus of textural information and the interpolation of spectral values, the impact of the pansharpening procedure on the bathymetry extraction was investigated by examining a dataset with no pansharpening, at 2 m resolution (Figure 3(A)), and a pansharpened dataset, at 0.5 m resolution (Figure 3(B)).

2.2.3. Atmospheric Correction

Atmospheric gases, aerosol particles and water vapor interact with electro-magnetic radiation (EMR), resulting in a decrease in transmission as a function of wavelength. However, for scientific purposes, the atmospheric correction can be either highly advocated (e.g., modeling the benthic albedo) or, conversely, discarded where a single image is being analyzed. The influence of the atmosphere on the measured signal tends to sharpen the image, facilitating the benthic classification, but this sharpening is likely to exacerbate spatial discontinuity/artifacts of the spectral relationships, contributing to reduce the quality of the bathymetry extraction model.

Figure 3. Representative example of the Gram-Schmidt spectral pansharpening method, supported by the spectral response function of the WorldView-2 (WV2). This method transformed the (**A**) 2-m initial multispectral dataset into a (**B**) 0.5-m multispectral dataset based on the 0.5-m initial panchromatic dataset, while preserving spectral patterns. Solid, dashed and dotted lines represent the mean, the standard deviations and the extremes of the spectral signatures of the subset area, respectively.

Atmospheric correction is actually considered as the second step of the radiometric correction, following the radiance calibration. The goal of this procedure is to transform the at-sensor radiance into ground/water-leaving radiance. However, for the sake of generalization, the atmosphere-corrected data are commonly expressed as the ratio between ground/water-leaving radiance and downwelling irradiance entering ground/water, called remote sensing reflectance (Rrs).
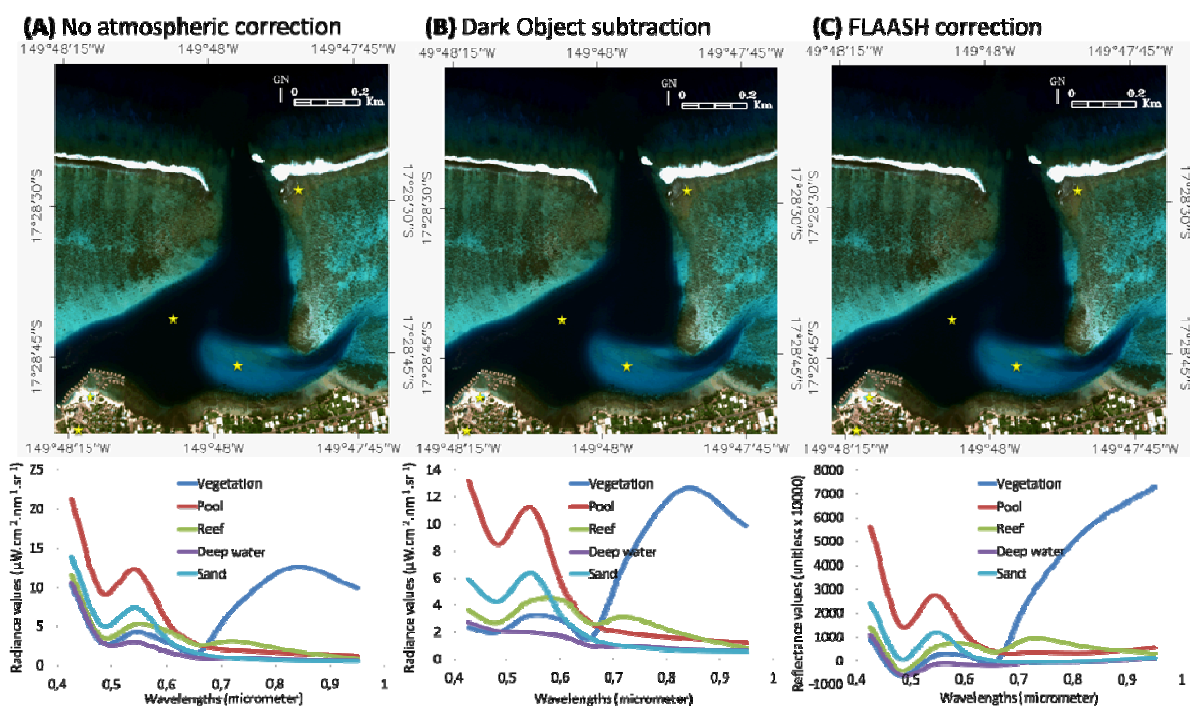
Procedures for atmospheric correction adopt either a one-way approach, retrieving the influence of atmospheric constituents, or a two-way method, retrieving constituents and resolving the radiation transport equation. While the atmospheric effect can be assessed by a dark subtraction (typically over dark land or deep clear water), the radiation transport can be elucidated by complex algorithms such as the MODerate resolution TRANsmittance (MODTRAN). The MODTRAN4 consists of the core of the Fast Line-of-site Atmospheric Analysis of Spectral Hypercubes (FLAASH) package [21]. Based on a standard radiation transport model, FLAASH assumes a flat Lambertian surface but is able to account for adjacency effects (radiation measured that is reflected from the object and then scattered by the atmosphere) for homogeneous areas [9]. Parameterization of the FLAASH and inner MODTRAN4 algorithms fine-tuned the two-way atmospheric correction (Table 2), defining, among others, a tropical atmosphere over a maritime area and using the discrete-ordinate-method radiative transfer (DISORT) with multiple-scattering option (detailed in Stamnes *et al.* [22]). However, neither the water nor the aerosol retrieval could be performed because the longest WV2 wavelength, centered at 950 nm, was

clearly inferior to the infrared wavelength recommended by Kaufman *et al.* [23]. The resulting water column value of MODTRAN4 was calculated and set to 4.11 g·cm^{-2}.

Table 2. Parameter values for the MODerate resolution TRANsmittance (MODTRAN)4-driven Fast Line-of-site Atmospheric Analysis of Spectral Hypercubes (FLAASH) module.
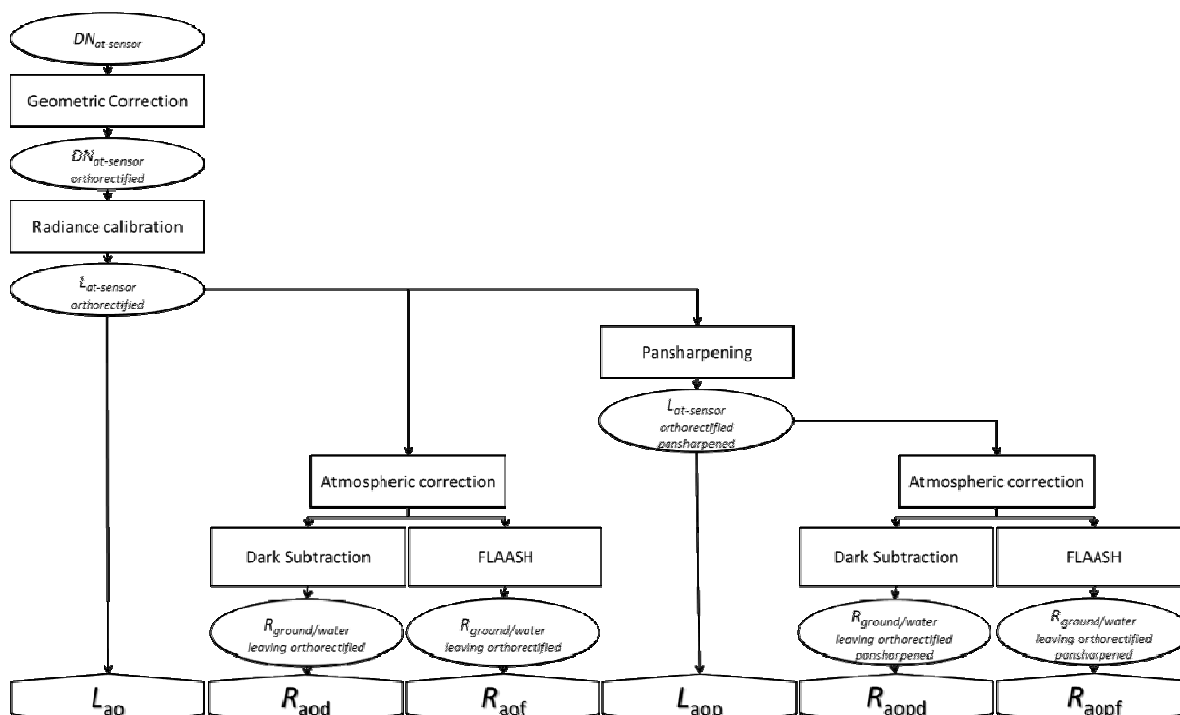
Altitude (km)	770
Ground Elevation (km)	0
Pixel size (m)	2/0.5
Flight Date	17 March 2010
Flight Time (GMT)	20 h 13 min 3 s
Atmospheric model	Tropical
Aerosol Model	Maritime
Aerosol Retrieval	None
Initial Visibility (km)	40
Aerosol Scale Height (km)	1.5
CO2 Mixing Ratio (ppm)	390
Square Slit Function	None
Adjacency Correction	Yes
MODTRAN Resolution (cm^{-1})	15
MODTRAN Multiscatter Model	Scaled DISORT
Number of DISORT Streams	8

Figure 4. Three modalities regarding the atmospheric correction have been retained: (**A**) none; (**B**) empirical Dark object Subtraction (DS); and (**C**) analytical FLAASH correction. Lower plots represent spectral signatures of five features (golden stars over images) against the three modalities.

In the current work, we tested the influence of the atmospheric correction on the bathymetry retrieval. Three modalities were retained: no atmospheric correction, dark object subtraction as the one-way correction, and rigorous two-way correction with the MODTRAN4-driven FLAASH algorithm (Figure 4). Taking into account the impact of how pansharpening was analyzed, our protocol spans six datasets (Figure 5).

Figure 5. Conceptual flowchart of the experimental approach aiming at optimizing the bathymetry retrieval with respect to two spatial resolutions (no pansharpening and with pansharpening) and three atmospheric corrections (none, empirical dark object subtraction and analytical FLAASH procedure).

2.2.4. Bathymetry Retrieval

The water column strongly interacts with EMR by modifying its direction and propagation. The change in direction is measured by an angle directly proportional to the refractive index of the medium, as stipulating by Descartes' law. As a function of the wavelength, EMR propagation is disturbed by water molecules, organic and mineral matter. The optical spectrum undergoes scattering and absorption mechanisms, exponentially attenuating EMR with water depth with respect to an increasing coefficient (the so-called diffuse attenuation) from purple to the near-infrared. This phenomenon is clearly expressed by the equation relating the radiance (at-sensor or water-leaving), the water depth, and the benthic albedo [11]:

$$R = (A_b - R_\infty)e^{-2kz} + R_\infty \tag{1}$$

where R is the radiance associated with one pixel, A_b is the benthic albedo, R_∞ is the radiance over a hypothetical optically deep water column (typically >60 m depth in the study area's waters) to avert the skew due to the benthic-associated albedo, k is the diffuse attenuation coefficient, and z is the

height of the water column. The wavelength terms inherent to R, A_b, R_∞, and k parameters are omitted for clarity.

Elucidating the bathymetry, z, requires rearranging (1) and solving for A_b. However, an empirical approach avoids solving for the latter parameter and estimates the bathymetry by correcting for albedo using a ratio of two wavelengths (or wavebands in our study) [24]. Although this method demonstrated satisfactory results for localized areas, Stumpf *et al.* [15] stressed that the constraint on this method is that five parameters need to be empirically determined, which either turns out to be time-consuming or demands potentially unrealistically strong assumptions of spatial homogeneity. Because the purpose of this work was to define an optimal combination of spectral bands for the bathymetry retrieval, we sought an algorithm providing an optimal trade-off between proficiency and simplicity. The ratio transform proposed by Stumpf *et al.* [15] adequately responded to the selection criteria. Endowed with capabilities of retrieving bathymetry over variable benthic types, even the darker ones relative to R_∞, and requiring a unique parameter to adjust, the ratio transform was solved for bathymetry as follows:
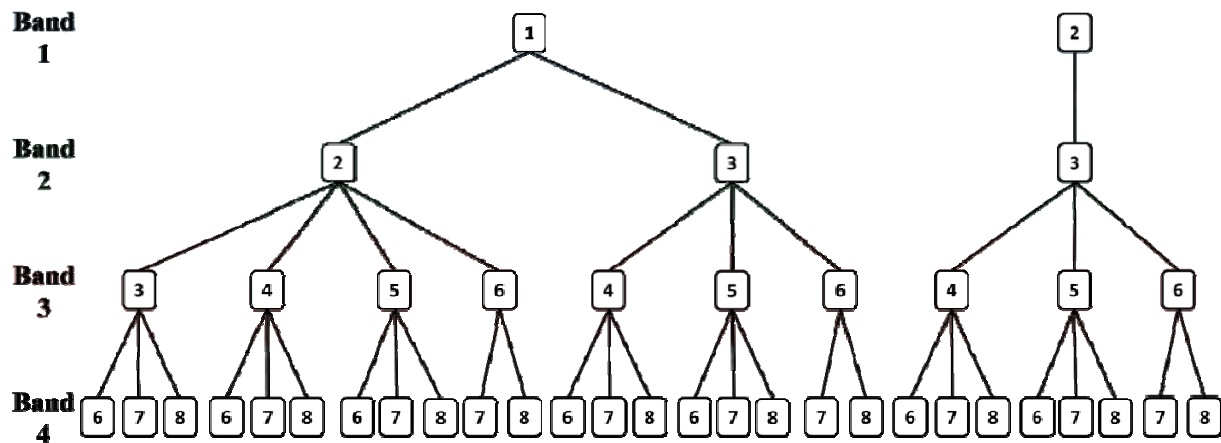
$$z = m_1 \frac{\ln{(nR_i)}}{\ln{(nR_j)}} - m_0 \tag{2}$$

where R_i and R_j refer to radiances of wavebands i and j, respectively, m_1 is an adjustable function allowing the ratio to be depth-scaled, n is a fixed constant ensuring the natural logarithm to be positive, and m_0 is the offset. Since the tidal level in Moorea varies within the bathymetric accuracy (<0.2 m), m_0 was fixed at 0.

The underlying principle of the ratio transform is that depth-driven change is significantly larger than the corresponding benthic albedo-driven change. Stumpf *et al.* [15] built and used the ratio transform with two IKONOS wavebands, characterized by differential water attenuation. We extended the methodology by employing the ratio transform for four various wavebands. Based upon the per-pixel result of the ratio transform, Digital Relative Depths Models (DRDM) were calculated at 2 m (514 × 568 floating points) and 0.5 m resolution (2,053 × 2,269 floating points).

2.3. Spectral Combinations

The novelty of the spectral capabilities of WV2 imagery was fully exploited in testing of all possible combinations as datasets intended for bathymetry retrieval. The ratio transform algorithm integrated four wavebands displaying four various diffuse water attenuation coefficients, sorted from the smallest to largest. Some constraints were applied when building the spectral datasets. Given the decreasing difference between coefficients, the first band, among the four encompassed in the spectral combination, was either purple or blue WV2 wavebands; the second band was either blue or green; the third band comprised green, yellow, red and NIR1 (very near-infrared), while the fourth and last band encompassed WV2 wavebands ≥725 nm (*i.e.*, near-infrared). For each of the modalities of spatial resolution (measured 2 m and pansharpened 0.5 m) and atmospheric correction (none, empirical dark object subtraction and analytical FLAASH correction), an array of 27 band combinations was subject to the bathymetry retrieval procedure. The spectral combinations can be illustrated with a flowchart (Figure 6). A total of 162 (=27 × 6) DRDM were thereby carried out to be tested against the *in situ* bathymetry measurements.

Figure 6. Flowchart of the spectral band combinations tested. The six test modalities (spatial resolution and atmospheric correction) encompassed 27 spectral combinations composed of four different bands.
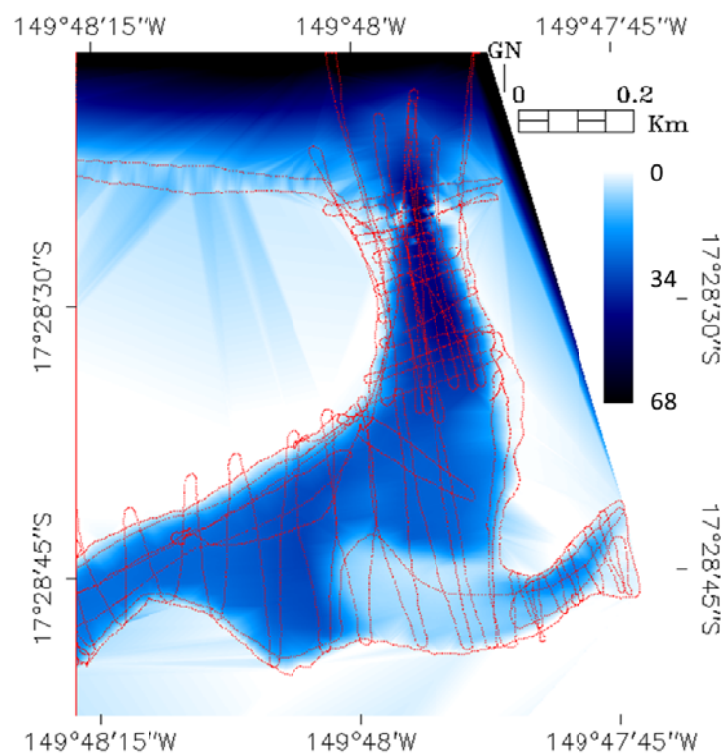

2.4. Acoustic Ground-Truthing

The robustness of the DRDM was defined using an acoustic survey that was conducted during 4–18 January 2011 over the study area. Depth measurements were made from a small boat equipped with a dual frequency (50/200 kHz) digital sonar and 12 channel GPS receiver (Garmin GPSMAP 546 s). Data were recorded at 0.5 Hz to a laptop as NMEA text strings. The boat made transects across the study region (Figure 7) at a nominal speed of 1 m/s, spanning the full range of depths and substrate types. Water column measurement accuracy was estimated to be <0.2 m.

A set of 8,489 individual measurements was used to calibrate (*cf. m_l* within Equation (2)) the DRDM and ultimately convert them into Digital Absolute Depths Models (DADM). The water depths surveyed ranged from 0 to 67.09 m (mean = 14.12, variance = 104.25, skewness = 0.75, and kurtosis = 0.54). The 8,489 floating points were linearly interpolated to build two Digital Ground-truth Depth Models (DGDM, one at 2 m and one at 0.5 m resolution), suitable to be stacked as a layer into the DRDM datasets (Figure 7). However, this rasterization was undertaken only to gain time in rapidly extracting the monitored 8,489 points of interest, and not to employ it where pixel values were interpolated. The consistency between DGDM and DRDM was quantified with a Pearson product-moment correlation coefficient (*r*) and attendant *p*-value (*i.e.,* the observed significance probability of obtaining a greater F-value by chance alone if the linear model fitted no better than the overall response mean). After sorting the matrix of 8,489 instances × 163 attributes by DGDM values, we computed *r* across the water depth. We got thereafter 66 *r*: the first computed corresponding to all ground-truth values (until 67 m), the second computed corresponding to ground-truth values topped at 65 m, the third computed corresponding to ground-truth values topped at 64 m, *etc.* While gradually reducing the dataset, this approach enabled the most efficient spectral combinations, regarding the bathymetry retrieval, to be discriminated and furthermore the depth range where they are the most robust. This "downscaling" analysis provided an optimal combination of spectral combinations, each of these specific to retrieving the bathymetry in a delineated depth window at 1 m resolution. The

spectral combinations providing the three best correlations with the DGDM were further examined in searching for the best statistical relationships using various fitting models and associated Root Mean Square Error and R^2adjusted. While R^2 measures the proportion of the variation around the mean explained by the fitting model, R^2adjusted adjusts the R^2 value to make it more comparable over models with different numbers of parameters by using the degrees of freedom in its computation. Root Mean Square Error estimates the standard deviation of the remaining variation which is not explained by the fitting.

Figure 7. Digital Ground-truth Depth Model (DGDM) linearly interpolated from the 8,489 acoustic soundings, represented in red points.

3. Results

3.1. Performance of the Spectral Band Combinations

From the inspection of the six scatterplots describing the correlation of the 162 DRDM and the DGDM, some patterns can be discerned (Figure 8). Since the correlation was calculated in a decreasing way, we examined results from the deepest to the shallowest bathymetry. While most of the spectral combinations appeared relatively steady from 67 m to 34 m, displaying a plateau, they then adopted either a gentle increase or a gentle decline until 10–20 m, they showed a significant decrease around 5 m, and finally increased until 1 m. We underscore that the various qualifications of the monotonicity (either increasing or decreasing) related to correlation curves were transformed into absolute values, given the interpretation of the Pearson's correlation in this study (Table 3). The best punctual performance was attributed to the spectral combination involving the purple, green, red and NIR2 (1357, $|r| = 0.85$, *p*-value < 0.001). However, this score was reached for a water depth of only 1 m. The second best performance (>1 m depth) was achieved using the purple, green, yellow and

NIR3 combination (1348) for a water depth of 14 m ($|r|$ = 0.77, *p*-value < 0.001). Conversely, the spectral combinations involving purple, blue, green and NIR3 (1238), purple, blue, yellow and NIR3 (1248), purple, blue, red and NIR3 (1258), purple, blue, NIR1 and NIR3 (1268) displayed the poorest performance at 1 m depth ($|r|$ = 1.25×10^{-16}, NS). Regarding the average performance across the water depth gradient, the best correlation was reached by the purple, green, yellow and NIR3 combination (1348, $|r|$ = 0.63), while the worst correlation was obtained from the purple, green, NIR1 and NIR3 combination (1368, $|r|$ = 0.08). This overall description necessitated a refinement in the analysis, taking into account the influence of the spatial resolution and atmospheric correction.

Table 3. Pearson product-moment correlation coefficients (*r*) of the best and worst averaged and performance of the bathymetry retrievals against spatial resolution and atmospheric correction.
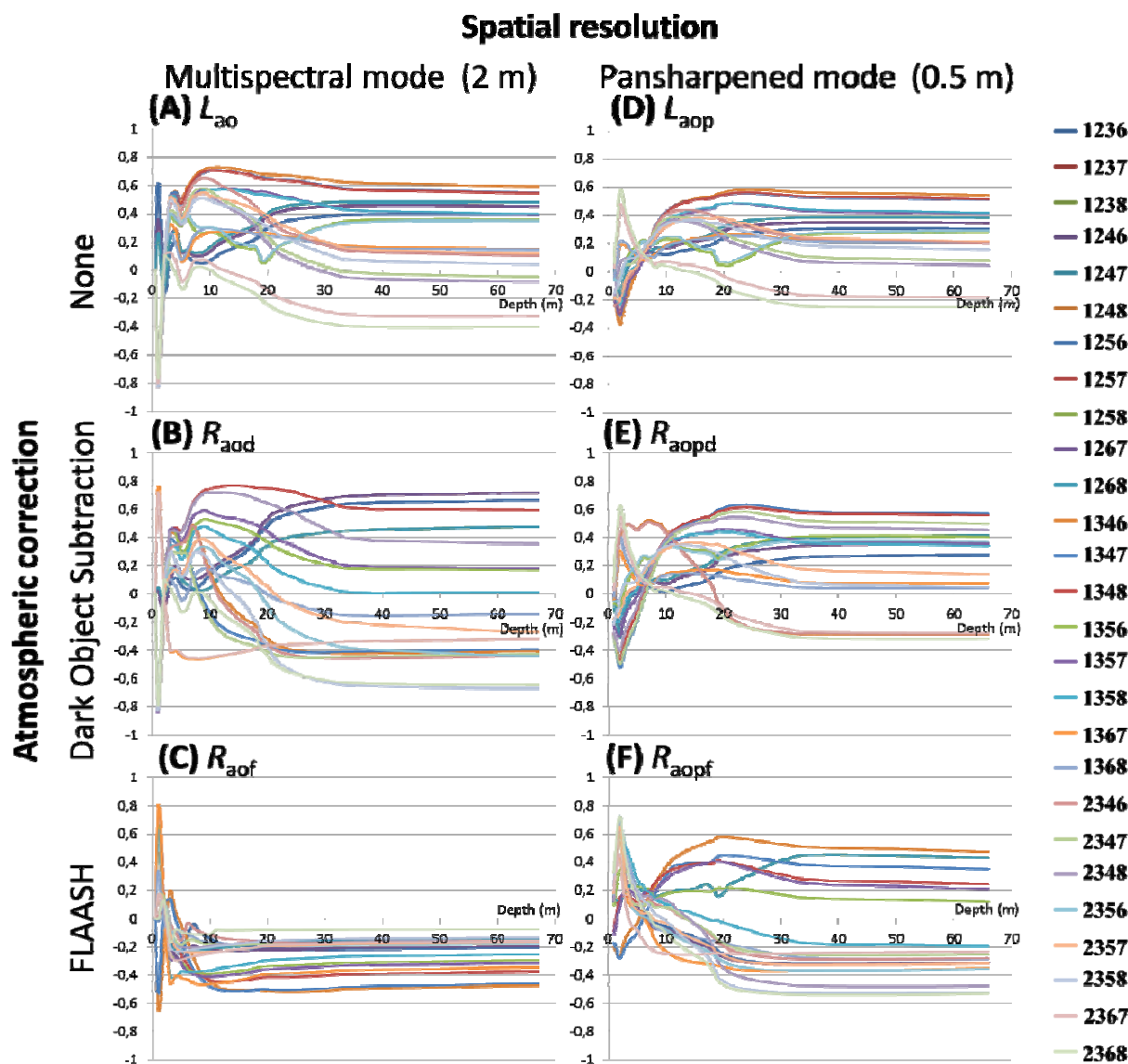
		No Correction		Dark Object Subtraction		FLAASH	
		2 m	**0.5 m**	**2 m**	**0.5 m**	**2 m**	**0.5 m**
Averaged	**Maximum**	0.63	0.5	0.63	0.53	0.46	0.46
	Minimum	0.16	0.13	0.13	0.08	0.08	0.16
Punctual	**Maximum**	0.84 ***	0.58 ***	0.85 ***	0.63 ***	0.81 ***	0.73 ***
	Minimum	5.78×10^{-4}	1.89×10^{-3}	4.81×10^{-4}	1.38×10^{-3}	1.25×10^{-16}	2.21×10^{-4}
		(NS, *p* = 0.95)	(NS, *p* = 0.92)	(NS, *p* = 0.97)	(NS, *p* = 0.94)	(NaN)	(NS, *p* = 0.99)

NB: *** means *p*-value < 0.0001, NS means No Significance (*p*-value >0.01), and NaN means Not a Number owing to the constant value of one the two variables to be correlated.

3.1.1. Influence of Spatial Resolution on Bathymetry Retrieval

A global trend of decreasing correlations was identified when the spatial resolution was enhanced from the measured 2 m to the pansharpened 0.5 m. For most spectral combinations, focusing on the most proficient ones, both the 67–34 m plateau and the 34–10/20 m trend had a decline in performance. This overall trend was suggested by a pattern of attraction towards zero (Figure 8). While the 2 m best correlations were 0.85 (1357 combination at 1 m depth) and 0.63 (1348 combination), punctually and averagely, respectively, they topped at 0.73 (2358 combination at 2 m depth) and 0.53 (1347 combination) when the bathymetry was retrieved from the 0.5 m DRDM. Regarding the minima, the water depth-averaged correlations bottomed at 0.08 for both spatial resolutions, while the lowest punctual results were attributed to the 2 m retrievals (1238, 1248, 1258 and 1268 combinations at 1 m depth). However, the lowest results derived from both spatial datasets might be considered as null (*i.e.*, 0.00). In addition, the fluctuating correlation curves resulting from the significant decrease pointed out before (*i.e.*, greater than) 5 m, turned into a nexus for the high resolution mode. From this minimum (close to zero), correlation curves continued fluctuating for the 2 m datasets, while they clearly increased (seemingly fitted with an exponential model) to peaks akin to 2 m, in the 0.5 m modalities. Interpretation of the spatial influence fairly suited with the first two atmospheric modalities (*i.e.*, none and dark object subtraction) but not satisfactorily with the rigorously corrected dataset (*i.e.*, FLAASH). Although the 5 m nexus was more highlighted and the 2 m peaks were lower in the 0.5 m mode, the 34–10/20 m trend and the 67–34 m plateau leveraged significant greater correlations (*sensu stricto* not in absolute values) than those stemming from the 2 m mode. This assessment encouraged us to decipher the impact of the atmospheric correction.

Figure 8. Scatterplots of Pearson product-moment correlation coefficients (*r*) computed between models of bathymetry retrieval and acoustic ground-truth measurements as a function of the maximal water depth. The 27 spectral combinations (series) used as bathymetric model inputs were analyzed with respect to spatial resolution and atmospheric correction. In the measured mode (2 m resolution): (**A**) no atmospheric correction for L_{ao}; (**B**) empirical dark object subtraction for R_{aod}; (**C**) analytical FLAASH correction for R_{aof}. In the pansharpened mode (0.5 m resolution); (**D**) no atmospheric correction for L_{aop}; (**E**) empirical dark object subtraction for R_{aopd}; (**F**) analytical FLAASH correction for R_{aopf}.

3.1.2. Influence of the Atmospheric Correction on Bathymetry Retrieval

Correcting the atmosphere through the empirical dark object subtraction procedure led to improved bathymetry retrievals. Visual inspection of Figure 8 showed a significant divergence of the correlation curves from zero. This gain appeared more prominently in the 2 m than in the 0.5 m datasets. Both averaged and punctual maxima concurred with this analysis, increasing from 0.62 to 0.63 and from 0.84 to 0.85. Despite the lower correlations, averaged and punctual gains turned out to be greater in the

0.5 than in the 2 m datasets (from 0.5 to 0.53 and from 0.58 to 0.63, respectively). While the averaged minima fell from 0.16 to 0.08, the punctual minima stagnated at 0.00.

On the other hand, rigorously correcting the atmospheric impact using the analytical FLAASH procedure substantially undermined the retrieval of bathymetry. This loss of performance was unambiguously illustrated by the (re-)attraction of the correlation curves towards 0, clearly evident in the 2 m dataset. Maxima statistics derived from the 2 m dataset corroborated the visual analysis, diminishing from 0.63 to 0.46 and from 0.85 to 0.81, for averaged and punctual datasets. Even if the averaged maxima diminished from 0.53 to 0.46, the 0.5 m dataset allowed the punctual maximum to increase from 0.63 to 0.73. Following the same blueprint as maxima, averaged minima declined in the 2 m dataset (0.13 to 0.08) and augmented in the 0.5 m dataset (0.08 to 0.16), while punctual minima all neighbored zero, regardless of the modalities.
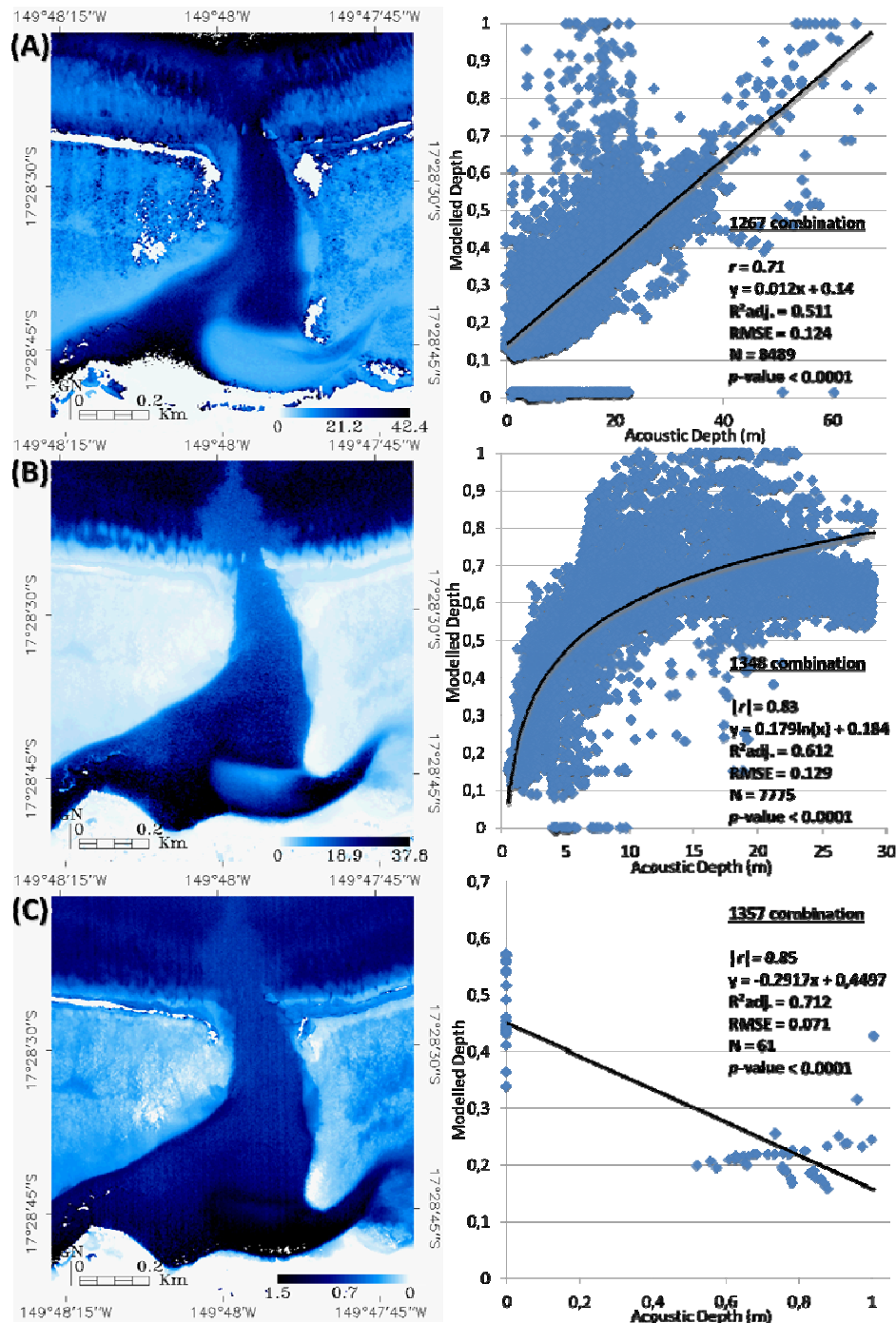
3.2. Mapping the Bathymetry Using the Best Spectral Band Combinations

Searching for the modality yielding the most efficient bathymetry retrieval, we used the best spectral combinations within the R_{aod} modality, *i.e.*, the original 2 m with a dark object subtraction by way of atmospheric correction. Topping the correlation curves, three spectral combinations succeeded one another across the water depth gradient (Figure 8(B)).

From 67 to 30 m depth, the correlation inherent to the 1267 combination, involving the purple, blue, NIR1 and NIR2 bands slightly decreased from 0.71 to 0.67 (Figure 8(B)). From all measurements (*i.e.*, 8,489 soundings), a linear model well explained the 1267-DRDM values and the corresponding DGDM data (R^2adj. = 0.51, Figure 9(A)). While the model reproduced actual depths up to approximately 20 m, a threshold around 25 m indicated the failure of the prediction. However, from 25 to 40 m, the same linear regression retrieved again meaningful water depths. The spatialized DRDM was calibrated with such an equation to build a DADM. The 1267-DADM, deemed the deep DADM, showed that spurs-and-grooves, visually revealed by two consecutive levels, and even the outer sandy spread (darkest feature off-shore) could be unraveled. Conversely, reefscape elements just above and under the water surface such as emerged and very shallow reefs with active wave breaking (seen as white zones inside the water body) were not elucidated by the model.

From 29 to 2 m depth, the correlation curve specific to the 1348 combination (*i.e.*, purple, green, yellow and NIR3 bands) outperformed the 1267 curve. Increasing from 0.67 to 0.77 (14 m), the correlation dramatically fell from 10 to 3 m, nearly 0.45 (Figure 8(B)). Interestingly, for *r* values less than or equal to one, the correlation neighbored the best values (|*r*| = 0.83). The relationships between the 7775 points defined in the two-dimensional 1348-DRDM/DGDM space were correctly translated by a natural logarithmic model (R^2adj. = 0.61, Figure 9(B)). Although the model adequately followed the crescent-like patterns of the data cloud, the scattering around it gradually increased with water depth, and especially from 15 m. Compared to the previous DADM, the 1348-DADM, called the intermediate DADM, substantially refined shallower reefscape features such as the furrowed platform, the reef crest, surge channels, the barrier and fringing reef flats. Water surface discrepancies noticed in the previous DADM were circumvented by this model. However, the improvements emerged at the expense of rendering spur-and-groove features and the outer sandy spread.

Figure 9. Digital Absolute Depth Models (DADM) and scatterplots of the ground truth acoustic measurements expressed as a function of the modeled water depths (R_{aod}: 2 m and dark object subtraction), resulting from (**A**) the 1267 (purple, blue, NIR1 and NIR2) spectral combination; (**B**) the 1348 (purple, green, yellow and NIR3) spectral combination; and (**C**) the 1357 (purple, green, red and NIR2) spectral combination.

For the 1 m depth, the 1357 combination, based on the purple, green, red and NIR2 bands, displayed the highest absolute correlation ($|r| = 0.85$, Figure 8(B)). Negatively sloped, a linear function robustly modeled the relationships between the 1357-DRDM and corresponding DADM values (R^2adj. = 0.71, Figure 9(C)), based on 61 points. In this respect, the scatterplot showed two clouds, one lying on the ordinate axis and the other one more erratic between 0.5 and 1 m, which were linked by

the linear model. Despite the negative model, the color ramp of the DADM matched those of both previous DADMs for the sake of readability. Bound by 0 and 1.5 m, the DADM, called the shallow DADM, put the emphasis on the extremely shallow reefscape elements, such as the reef crest, the barrier and fringing reef flats punctuated with micro-atolls. Since the model was selected for its performance between 0 and 1 m, modeled water depths seaward the reef crest and within the channel (both globally rendered in darker tones) did not retrieve actual bathymetry.

4. Discussion

4.1. Differential Contributions of the Pansharpening and Atmospheric Corrections

Testing the respective influence of spatial resolution and atmospheric correction on bathymetry retrieval addressed recurrent questions that are important when using spaceborne passive multispectral remote sensing for reefscape characterization. The bathymetry retrieval globally diminished with spatial resolution. In addition, the so-called nexus around 5 m strongly determined the influence of the enhancement of the spatial resolution. This blueprint corroborated previous work by Adler-Golden *et al.* [9], who pointed out that the systematic error reached a maximum at around 6 m depth. The loss of consistency with ground-truthing might result from the pansharpening procedure. This approach scaled up considerably more relevant information about textural gradients for the multispectral dataset but did not elucidate spectral measurements at the panchromatic spatial resolution. While being very useful for refining spatial variations of features detectable in the panchromatic range, the pansharpening method failed to assign absolute values to features not or poorly captured by all spectral bands. Based on the band ratio, the products of the transform did not account for subtle spectral variations (decisive for distinguishing benthic from water column contribution) and were unavoidably less proficient to those stemming from originally measured bands. Typically, the water depth over coral colonies whose pigments interacted with purple EMR (not comprised into the panchromatic range) and whose diameter was <2 m was highly susceptible to be inconsistent with reality. However, retrieving bathymetry using the pansharpening method might be advocated for some spectral combinations, showing sizable congruency with ground-truthing (e.g., 1346, 1347, 1348 and 2368 whose correlation was >0.5). As discussed above, mapping bathymetry at higher spatial resolution would have to be conducted over benthic features that interact with all the bands comprised into the panchromatic range, such as *Porites lobata*, whose detection was enhanced by spectral indices involving green, yellow and red bands [7]. Note that the 1347 and 1348 best performances in the 0.5 m datasets occurred for a specific atmospheric correction, namely dark object subtraction.
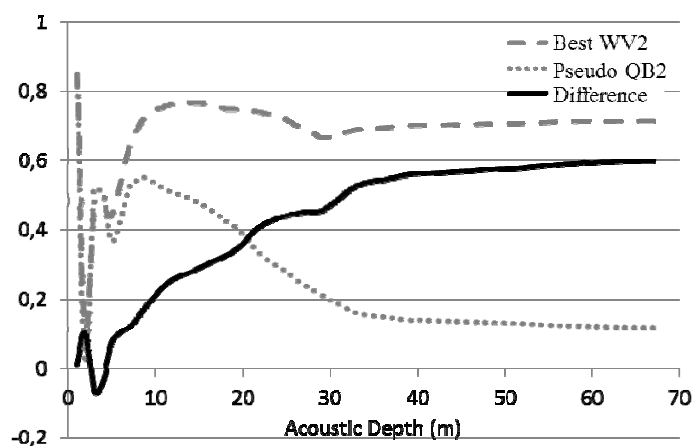
The agreement between modeled and actual depths varied as a function of the atmospheric correction. While no correction and dark object subtraction provided similar patterns of correlation curves against water depths (in favor of the dark subtraction), the FLAASH correction yielded exclusively negative correlations (slightly lower, in absolute numbers, than those issued from none) except for very shallow water depths, which were positive. Rigorously correcting the atmospheric influence, through an analytical procedure, was intuitively expected to yield the best performance for handling water-leaving Rrs, and thus for optimally retrieving bathymetry. However, the rigorous correction was surpassed by both no correction and the empirical approach, dark object subtraction. A

reason why this correction performed poorly might pertain to the fact that the FLAASH package was robust over bright objects (typically, land) but was not so proficient over darker objects (typically, underwater). Other rigorous atmospheric algorithms should be tested, such as Tafkaa [25], to evaluate their improvement of correction over water bodies. Despite the recognized accuracy of atmospheric procedures, Rrs products have remained likely due to significant errors arising from radiometric calibration of the sensor [9,26]. Processing radiometric errors by applying a simple offset, computing from the minimum Rrs values (water-leaving radiances) for each spectral channel, enabled Adler-Golden *et al.* [9] to successfully correct FLAASH images (in the same way as the dark object subtraction is treated the at-sensor radiances). Another alternative might use spectral polishing consisting of a uniform linear transformation aiming at removing spectral artifacts by employing reference pixels from which band-dependent gain factors and offsets could be calculated [27]. Designed for hyperspectral datasets, these further analyses require that artifacts conveyed by the broadness of the WV2 multispectral bands are taken into account. Finally, in the case where a punctual study without attempt of spatio-temporal comparisons is planned, it is recommended to retrieve the bathymetry directly from imagery deprived of atmospheric correction (*i.e.*, at-sensor radiance) given the consistency highlighted above.

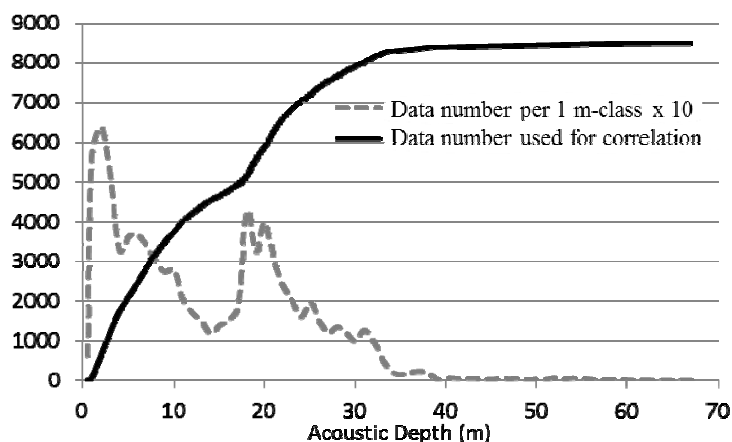### 4.2. Spectral Enhancement Implied a Refinement of the Bathymetry Retrieval

Integrating the novel bands derived from the WV2 imagery enhanced the bathymetry retrieval in tropical clear water using the ratio transform approach. Based on the four bands inherent to either QB2 or IKONOS, the bathymetry was resolved up to 20 m ([9] and [15] respectively). The three visible and one NIR bands pertaining to the two latter sensors could be related to the WV2 2357 combination (namely, blue, green, red and NIR2). The best performance showed by the pseudo QB2 combination was found within the 2 m/no atmospheric correction modality (L_{ao}). From the 67 to 34 m, the plateau slightly increased from 0.11 to 0.15, then rapidly grew to 9 m, meeting 0.55, momentarily fluctuating between 0.54 and 0.37 to 3 m, and finally topped at 0.84 (in absolute values) at 1 m. An inflection point visible at 20 m may concur with both above-cited works. However, using the four novel WV2 bands (purple, yellow, NIR1 and NIR3), the bathymetry retrieval was strongly refined relative to the pseudo QB2 results: from 67 to 30 m, the WV2 1267 combination varied between 0.67 and 0.71, from 30 to 3 through 14 m, the WV2 1348 combination met 0.67, 0.77 and 0.44, respectively, and finally the WV2 1357 combination reached 0.85 (in absolute values) at 1 m. Those results stemmed from the 2 m/dark object correction modality (R_{aod}). We thereafter compared L_{ao} 2357 (pseudo QB2) and R_{aod} 1267/1348/1357 spectral combinations so that the gain conveyed by the WV2 four novel bands can be accurately quantified (Figure 10). Except for 3 and 4 m, the best WV2 combination systematically outperformed the pseudo QB2 results, gaining a high increase in correlation values from 4 to 34 m (from 0 to 0.54, respectively) and a more moderate growth from 34 to 67 m (from 0.54 to 0.6). The overall accuracy, close to 1 m, might be assumed as the effect of the noise integrated into the EMR measurement, detectable as random variance within 1 pixel lag. Since we found the two most sharply contrasted average performances to within one spectral band of difference (1348, $|r| = 0.63$ and 1368, $|r| = 0.08$), we suggest that the selection of bands played a crucial role in subsequent retrievals.

Figure 10. Absolute Pearson product-moment correlation coefficients (*r*) as a function of water depth as computed between the best WV2 R_{aod} model (composed of the 1267 (purple, blue, NIR1 and NIR2), the 1348 (purple, green, yellow and NIR3) and the 1357 (purple, green, red and NIR2) spectral combinations); the pseudo QB2 L_{ao} model (2357 (blue, green, red and NIR2) spectral combination); and their difference.

The primary results of this study targeted the potential for considerable deepening of the water depth penetration relative to previous studies. Even though we obtained a correlation of 0.71 at a 67 m depth, it was more reasonable to find a robust explanation of this outstanding result. Considering the number of data points involved in the computation of the correlations shed light on the results (Figure 11). Correlations obtained from 67 to nearly 39 m were not well supported given the low data density (3.3 ± 1.6 points per 1 m-class). This assessment suggests that the correlation computed at 67 m was essentially driven by data ≤39 m. The good agreement (*r* = 0.7) at 39 m, resulting from the 1267 model, was supported by the corresponding scatterplot (Figure 9(A)) showing relative tight dispersion around the linear model, despite a more scattered phase centered between 20 and 25 m. From 39 to 2 m, overall increased data density per 1 m-class compensated for the reduction of data points used for computation, suggesting that correlations were statistically reliable. The robustness of the 1348 model (between 30 and approximately 7 m), indicated by the large number of data points used for the computation and the attached scatterplot and correlation curve, could warrant that the 30 m depth can be attained. Note that the trend of dispersion identified around 15 m (Figure 9(B)) in the latter model might be a consequence of low data density per 1-m classes, appearing as a groove between the two peaks of 20 and 2 m (Figure 11). Finally, since the correlation computed for 1 m encompassed only 61 data, the very high value found with the 1357 model should be cautiously interpreted, as Stumpf *et al.* [15], also found that the ratio transform yielded problematic results with water depths ≤0.6 m, and this merits further research.

Figure 11. Data points per 1 m-depth class (×10) involved to compute correlation coefficients across the water depth gradient.

4.3. Towards an Improved Solution for Benthic Albedo

Refining bathymetry over tropical reefscapes using spaceborne data enabled the geomorphic features to be quantified, such as the outer sandy patches, spurs-and-grooves, optically deep (>20 m) lagoon and reef pass channels. However, information about the benthic spectral characteristics is needed to undertake robust mapping. Various spectral signatures can determine the coral community structure as well as its state of health [7]. The enhancement of the bathymetry retrieval constitutes a great development aiming at improving the inversion of the underwater radiative transfer model. The linear ratio transform made the simplifying assumption of constant water optical properties within the scene. This avoids some ambiguities in separating the effects from different depths, benthic materials, and water types. However, considering the diffuse attenuation coefficient, *K*, to be constant over waters surrounding volcanic islands seems unlikely. Previous studies have advocated dividing *K* into a diffuse attenuation coefficient for downwelling light and a diffuse attenuation coefficient for upwelling light, itself divided into a coefficient for light originating from the benthos and a coefficient for light originating from each layer in the water column [28]. Recent inversion methods of the underwater radiative transfer model employed nonlinear techniques and obtained satisfactory retrievals using spectroradiometric field measurements necessary to link the Rrs with the current environmental conditions [29]. We point out upfront that remote sensing of reefscapes will not fully integrate decision-making flowcharts unless the benthic albedo can be reliably retrieved. Our premise is that the additional two visible (purple and yellow) and the NIR (NIR1) bands, in addition to enhancing the bathymetry retrieval, should be insightful for the discrimination of the structure and health of the reefscape communities, even colonies, and for change analyses, given the more comprehensive optical spectrum.

5. Conclusions

This study demonstrated the enhancement of the bathymetry retrieval in shallow coral reef waters using the WV2 spaceborne eight band imagery, and the ratio algorithm. The contribution of the spectral bands to the bathymetry retrieval and the influence of the pansharpening and atmospheric correction procedures were assessed by 8489 instances × 163 DDM (162 DRDM and 1 DGDM). The

reference bathymetry was acquired during a waterborne high resolution digital sonar survey. Three main outcomes emerged from our study. Increasing spatial resolution from 2 to 0.5 m led to a diminution of agreement between modeled and measured water depths, more sharply evidenced around the actual 5 m. Counter-intuitively, the analytical atmospheric correction provided poorer results than those stemming from no atmospheric correction and empirical dark object correction. When considered with this latter correction at the 2 m resolution, the purple, blue, NIR1 and NIR2 (WV2 1st-2nd-6th-7th bands), the purple, green, yellow and NIR3 (WV2 1st-3rd-4th-8th bands), and the purple, green, red and NIR2 (WV2 1st-3rd-5th-7th bands) spectral combinations furnished the greatest agreement with ground-truthing at actual 39 m ($r = 0.7$), 30 m ($r = 0.65$) and 1 m ($|r| = 0.85$), respectively. However, given the amount of data involved for the models' computation and related discrepancies pointed out, the intermediate 1348 model was deemed as the most reliable model attaining 30 m. Compared to the literature on spaceborne-derived bathymetric products, it represented an increase in depth penetration close to 10 m. This finding was reinforced by comparison with results derived from a simulated QB2, examined in this work. Gains of correlation of 0.47 and 0.36 were reckoned for depths of 30 and 20 m, respectively. The integration of the innovative WV2 spectral bands into the ratio algorithm therefore consists of a meaningful improvement for robustly characterizing reefscape features from spaceborne multispectral products. This enhancement can be combined with the best methods to determine the diffuse attenuation coefficient so that reefscape evolution, facing major disturbances, can be frequently updated at the colony-scale level.

Acknowledgements

References

1. Mumby, P.J.; Skirving, W.; Strong, A.E.; Hardy, J.T.; LeDrew, E.F.; Hochberg, E.J.; Stumpf, R.P.; David, L.T. Remote sensing of coral reefs and their physical environment. *Mar. Pollut. Bull.* **2004**, *48*, 219–228.
2. Guenther, G.C.; Brooks, M.W.; LaRocque, P.E. New capabilities of the "SHOALS" airborne lidar bathymeter. *Remote Sens. Environ.* **2000**, *73*, 247–255.
3. Isoun, E.; Fletcher, C.; Frazer, N.; Gradie, J. Multi-spectral mapping of reef bathymetry and coral cover, Kailua Bay, Hawaii. *Coral Reefs* **2003**, *22*, 68–82.
4. Louchard, E.M.; Reid, R.P.; Stephens, F.C.; Davis, C.O.; Leathers, R.A.; Downes, T.V. Optical remote sensing of benthic habitats and bathymetry in coastal environments at Lee Stocking Island, Bahamas: A comparative spectral classification approach. *Limnol. Oceanogr.* **2003**, *48*, 511–521.
5. Mishra, D.R.; Narumalani, S.; Rundquist, D.; Lawson, M.; Perk, R.J. Enhancing the detection and classification of coral reef and associated benthic habitats: A hyperspectral remote sensing approach. *J. Geophys. Res.* **2007**, *112*, C08014.

6. Mishra, D.; Narumalani, S.; Rundquist, D.; Lawson, M. Benthic habitat mapping in tropical marine environments using QuickBird multispectral data. *Photogramm. Eng. Remote Sensing* **2006**, *72*, 1037–1048.

7. Collin, A.; Planes, S. Highlighting three reef-building coral communities' health state using spectral diversity indices from WorldView-2 imagery. *Remote Sens. Environ.* **2011**, submitted.

8. Gianinetto, M.; Lechi, G. A DNA Algorithm for the Bathymetric Mapping in the Lagoon of Venice Using QuickBird Multispectral Data. In *Proceedings of the XXXVth ISPRS Congress*, Istanbul, Turkey, 12–23 July 2004; Paper 18.

9. Adler-Golden, S.M.; Acharya, P.K.; Berk, A.; Matthew, M.W.; Gorodetzky, D. Remote bathymetry of the littoral zone from AVIRIS, LASH, and QuickBird imagery. *IEEE Trans. Geosci. Remote Sens.* **2005**, *43*, 337–347.

10. Collin, A.; Chancerelle, Y.; Pouteau, R. The Reefscape Ecology in the Middle of the Southern Pacific: Confluence of the Polynesia Mana Network and Very High Resolution Satellite. In *Seascapes: Views and Actions*; French Agency of Marine Protected Areas, Ed.; Springer: Berlin/Heidelberg, Germany, 2011.

11. Lyzenga, D.R. Passive remote sensing techniques for mapping water depth and bottom features. *Appl. Opt.* **1978**, *17*, 379–383.

12. Philpot, W.D. Bathymetric mapping with passive multispectral imagery. *Appl. Opt.* **1989**, *28*, 1569–1578.

13. Lyons, M.; Phinn, S.; Roelfsema, C. Integrating Quickbird multi-spectral satellite and field fata: Mapping bathymetry, seagrass cover, seagrass species and change in Moreton Bay, Australia in 2004 and 2007. *Remote Sens.* **2011**, *3*, 42–64.

14. Lee, Z.P.; Carder, K.L.; Arnone, R.A. Deriving inherent optical properties from water color: A multiband quasi-analytical algorithm for optically deep waters. *Appl. Opt.* **2002**, *41*, 5755–5772.

15. Stumpf, R.P.; Holderied, K.; Sinclair, M. Determination of water depth with high-resolution satellite imagery over variable bottom types. *Limnol. Oceanogr.* **2003**, *48*, 547–556.

16. Hench, J.L.; Leichter, J.J.; Monismith, S.G. Episodic circulation and exchange in a wave-driven coral reef and lagoon system. *Limnol. Oceanogr.* **2008**, *53*, 2681–2694.

17. Adam, T.C.; Schmitt, R.J.; Holbrook, S.J.; Brooks, A.J.; Edmunds, P.J.; Carpenter, R.C.; Bernardi, G. Herbivory, connectivity, and ecosystem resilience: Response of a coral reef to a large-scale perturbation. *PLoS One* **2011**, *6*, e23717.

18. Maritorena, S.; Morel, A.; Gentili, B. Diffuse reflectance of oceanic shallow waters: Influence of water depth and bottom albedo. *Limnol. Oceanogr.* **1994**, *39*, 1689–1703.

19. González-Audícana, M.; Otazu, X.; Fors, O.; Alvarez-Mozos, J. A low computational-cost method to fuse IKONOS images using the spectral response function of its sensors. *IEEE Trans. Geosci. Remote Sens.* **2006**, *44*, 1672–1682.

20. Laben C.A.; Brover, B.V. Process for Enhancing the Spatial Resolution of Multispectral Imagery Using Pan-Sharpening. US Patent 6011875, 4 January 2000.

21. Matthew, M.W.; Adler-Golden, S.M.; Berk, A.; Felde, G.; Anderson, G.P.; Gorodetzky, D.; Paswaters, S.; Shippert, M. Atmospheric correction of spectral imagery: Evaluation of the FLAASH algorithm with AVIRIS data. *Proc. SPIE* **2003**, *5093*, 474–482.

22. Stamnes, K.; Tsay, S.-C.; Wiscombe, W.; Jayaweera, K. Numerically stable algorithm for discrete-ordinate-method radiative transfer in multiple scattering and emitting layered media. *Appl. Opt.* **1988**, *27*, 2502–2509.

23. Kaufman, Y.J.; Tanré, D.; Remer, L.A.; Vermote, E.F.; Chu, A.; Holben, B.N. Operational remote sensing of tropospheric aerosol over land from EOS Moderate Imaging Spectroradiometer. *J. Geophys. Res.* **1997**, *102*, 17051–17067.

24. Lyzenga, D.R. Shallow-water bathymetry using combined lidar and passive multispectral scanner data. *Int. J. Remote Sens.* **1985**, *6*, 115–125.

25. Montes, M.J.; Gao, B.-C. Improvements to the Tafkaa Atmospheric Correction Algorithm for Hyperspectral Ocean-Color Data. In *Proceedings of Hyperspectral Imaging and Sounding of the Environment*, Santa Fe, NM, USA, 11–15 February 2007; Paper HThA3.

26. Gao, B.-C.; Montes, M.J.; Ahmad, Z.; Davis, C.O. Atmospheric correction algorithm for hyperspectral remote sensing of ocean color from space. *Appl. Opt.* **2000**, *39*, 887–896.

27. Boardman, J.W. Post ATREM Polishing of AVIRIS Apparent Reflectance Data Using EFFORT: A Lesson in Accuracy *versus* Precision. In *Proceedings of Summaries of the 7th JPL Airborne Earth Science Workshop*, Washington, DC, USA, 12–16 January 1998; Volume 1, JPL Pub. 53.

28. Brando, V.E.; Anstee, J.M.; Wettle, M.; Dekker, A.G.; Phinn, S.R.; Roelfsema, C. A physics based retrieval and quality assessment of bathymetry from suboptimal hyperspectral data. *Remote Sens. Environ.* **2009**, *113*, 755–770.

29. Dekker, A.G.; Phinn, S.R.; Anstee, J.; Bissett, P., Brando, V.E.; Casey, B.; Fearns, P.; Hedley, J.; Klonowski, W.; Lee, Z.P.; *et al*. Intercomparison of shallow water bathymetry, hydro-optics, and benthos mapping techniques in Australian and Caribbean coastal environments. *Limnol. Oceanogr.: Methods* **2011**, *9*, 396–425.